BCSJ Award Article

Molecular Aggregation State and Electrical Properties of Terthiophenes/Imogolite Nanohybrids

Weng On Yah,[1] Atsushi Irie,[1] Nattha Jiravanichanun,[2] Hideyuki Otsuka,[1,2] and Atsushi Takahara*[1,2]

[1]Graduate School of Engineering, Kyushu University, 744 Motooka, Nishi-ku, Fukuoka 819-0395

[2]Institute of Materials Chemistry and Engineering, Kyushu University, 744 Motooka, Nishi-ku, Fukuoka 819-0395

Received March 9, 2011; E-mail: takahara@cstf.kyushu-u.ac.jp

Organic/inorganic nanohybrid materials composed of terthiophenes and imogolite were prepared by means of specific surface interaction between a phosphonic acid group in terthiophene derivatives and aluminol groups on the surface of imogolite. The new materials were investigated by FTIR, UV–vis absorption, fluorescence spectroscopy, TEM observation, nitrogen adsorption–desorption, and *I–V* measurement. Addition of terthiophene of phosphonic acid derivatives into imogolite brought some changes in absorption and photoluminescence spectra, suggesting the formation of H-type aggregate on imogolite surface. The analysis of UV–vis spectra and nitrogen adsorption–desorption data provided insight into the effect of molecular structure of terthiophenes on the adsorption and aggregation behaviors on the imogolite surface. In addition, a significant enhanced current flow was observed through imogolite film when imogolite was chemisorbed by electron-withdrawing terthiophenes. In contrast, current flow decreased as the electron-donating terthiophene was chemisorbed on imogolite. A possible mechanism for such phenomena is discussed.

Organic electronic devices made up from small molecules of dye neatly linked by self-assembly to solid support are vital components in light energy conversions systems, optical devices, and sensors.[1,2] The self-assemblies of molecules are widely found in nature, for instance, chlorophylls which are embedded in the thylakoid membranes of chloroplasts are specifically arranged in rod-shaped aggregate and act as an efficient light-harvesting system for photosynthesis.[3–6] Recently, there has been considerable research interest focused on the study of photo-physicochemical properties, aggregations, and absorption behavior of dye molecules on the surface of inorganic materials. These studies can provide invaluable information that serves as guidance for fabrication of high-performance dye-based electronic devices.[7–10] Such organic/inorganic hybrid nanomaterials of the dye/solid support aggregates are expected to demonstrate novel nanotechnological applications that the corresponding monomeric dye could not perform.[11,12] Nevertheless, the main challenge in this field remains preparation of a stable dye/solid support aggregate with adjustable aggregation structure on inorganic material surfaces.

Generally, most dye molecules can self-assemble and adsorb on inorganic material surfaces through simple physisorption. However, given the fundamental and practical significance of better control over the adsorption and aggregation state of dye molecules on solid support, many research groups are involved in the effort to synthesize novel dye structures with anchoring groups attached. The strategy of attaching anchoring group into the dye is very important, in a sense that one can adjust the distance of dye from the surface, controlling the aggregation state of dye, as well as for chemical surface modification.[9] Additionally, it is possible to graft a variety of functionalized and photoactive species (porphyrins, phthalocyanines, viologens, rhodamine B, naphthalenes, perylenes, fullerenes, and conjugated hydrocarbon) onto metal oxide surfaces of SiO_2, TiO_2, ITO, WO_3, and ZrO_2 in order to induce the formation of well-defined nanoscopic photoactive molecular arrays or better described as "heterosupramolecular assemblies." The heterosupramolecular chemistry concept introduced by Fitzmaurice et al. embraces both covalent and noncovalent interactions of condensed phase surfaces and molecular components.[13,14] Anchoring groups in this context play an important role in linking or replacing the molecular components within a supramolecular system with condensed phase to form heterosupramolecular assemblies. There are some well-studied anchoring groups for inorganic surfaces for instance, phosphonic acids, carboxylic acids, acid chlorides, esters, and amides. The best anchoring groups for inorganic material surface of metal oxides are phosphonates, followed by carboxylates and their derivatives. The phosphonates are reported to exhibit relatively high equilibrium binding constant and saturation surface coverage with pH-dependent reversible binding. Other anchoring groups of silanes, ether, acetylacetonate, and salicylates that able to form covalent bonds with

Published on the web August 23, 2011; doi:10.1246/bcsj.20110080

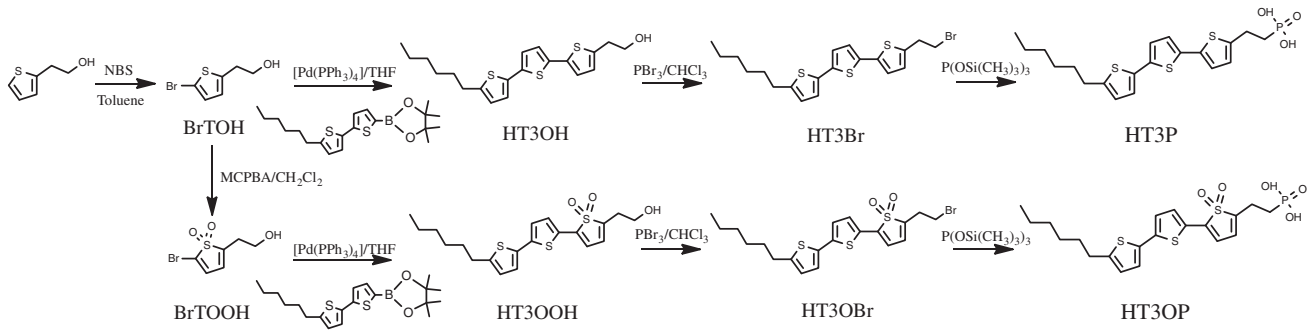

Scheme 1.

hydroxy groups of metal oxides surfaces have also been explored and studied for similar purposes.[15–19]

To study the adsorption and aggregation behavior of dye–inorganic hybrid material at molecular scale, we have chosen terthiophene derivatives as the molecular component and imogolite as the condensed phase for the construction of nanoscopic heterosupramolecular assembly. Imogolite was first discovered in 1962 from volcanic ash soil[20] and its chemical synthesis was developed in 1977.[21] Imogolite is a single wall aluminosilicate nanotube of ca. 2.5 nm external diameter and ca. 1.0 nm internal diameter with length up to 1 μm.[22] The empirical formula of imogolite can be described as $(OH)_3Al_2O_3SiOH$, which shows the atomic layer arrangement going from exterior to the interior of the tube wall. Due to its nanotubular morphology with full coverage of hydroxy groups, imogolite exhibits high surface area and acid reactivity. Imogolite can also form strong chemical bonds with heavy metal cations, phosphate,[23] arsenate, sulfate, and organic materials, as surface-adsorbed species in solution.[24] Although imogolite lacks intrinsic semiconductivity as those of TiO_2 or ITO, the unique nanotubular structure of imogolite does exhibit several properties that meet the requirements as an interesting condensed phase for heterosupramolecules system, e.g., high surface area for molecular component adsorption, abundant empty surface sites for covalent binding of acidic anchoring groups, and high stability against changing environmental conditions.[25] To render this one-dimensional material with semiconductivity, imogolite nanotubes have been functionalized with conjugated polymers of polypyrole[26] and polyphenylene.[27,28] The functionalized imogolite hybrid materials are expected to have many applications in molecular electronics and can be exploited as a cheap semiconducting material analogous to carbon nanotubes. On the other hand, oligothiophenes are an important group of π-conjugated compounds, characterized by homogeneous electronic structure and sharper photoelectric properties than that of polymer counterparts and thus have been widely investigated for a variety of promising industrial and scientific applications, such as field effect transistors (FETs), organic LEDs, liquid crystals (LC), photovoltaic cells, lasers, and biotechnology.[29–33] Unsubstituted oligothiophenes are electron-donating materials. However, chemical transformation by addition of oxygen to the sulfur of thienyl rings to form a thienyl-1,1-dioxide convert it into stable oligomer with enhanced electron affinity. This oligothiophene with electron-deficient thienyl-1,1-dioxide moieties inserted within the aromatic skeleton that shows both high electron affinity and ionization potential would find application as an attractive electron acceptor in photoluminescence and photovoltaics.[34–36] In the current study, both electron-donating and -accepting terthiophene of phosphonic acid derivatives (Scheme 1) were synthesized and employed as molecular components and their adsorption and aggregation state on imogolite were investigated.

Results and Discussion

FTIR Spectra Analysis. The chemisorptions of HT3P and HT3OP on imogolite surface in the hybrid material were identified by FTIR spectroscopy. Figure 1a shows the FTIR spectra of HT3P/imogolite hybrid, HT3P, and imogolite, and (b) of HT3OP/imogolite hybrid, HT3OP, and imogolite, respectively. Imogolite exhibits two bands, namely, the OH stretching frequency near 3500 cm^{-1} and the HOH deformation band at 1633 cm^{-1}, due to the presence of water inside the pore and external surface. There are also two bands at 997 and 943 cm^{-1} due to the Si–O–Al stretching modes that are indicative of the isolated orthosilicate units present in the imogolite structure.[22] In the spectrum of HT3P/imogolite hybrid, the spectrum showed the characteristic absorptions corresponding to HT3P at 2850–2950 cm^{-1} to the CH_2 stretching vibration. On the other hand, the large absorption at 2200–2500 cm^{-1} assigned to the OH stretching vibration of phosphonic acid groups has disappeared. The broadness of the peaks in the P–O region between 1200 and 900 cm^{-1} make it difficult to interpret, but the changes observed show that a strong interaction of the phosphonate headgroup with the imogolite surface is present.[37] Also, the disappearance of the band at around 1004 cm^{-1} was observed in the study of HT3P on imogolite. The absence of this band which can be assigned to P–O–H groups[38,39] was interpreted as an indication that HT3P molecules were chemisorbed onto the surface of imogolite nanofiber as illustrated in Figure 1c. Similar trends can also be observed from the FTIR spectrum of HT3OP/imogolite hybrid as shown in Figure 1b. The disappearance of P–O–H at around 1011 cm^{-1} indicating HT3OP molecules also underwent chemisorptions when in contact with imogolite. However, the definite assignment of these bands is difficult since it depends on the degree of hydrogen bonding or metal binding, and the ranges for the different P–O stretching peaks greatly overlap.[37]

UV–vis Absorption Spectra. To explore the optical properties of these oligothiophenes on imogolite surface, UV–vis spectra of terthiophenes (HT3P and HT3OP)/imogo-

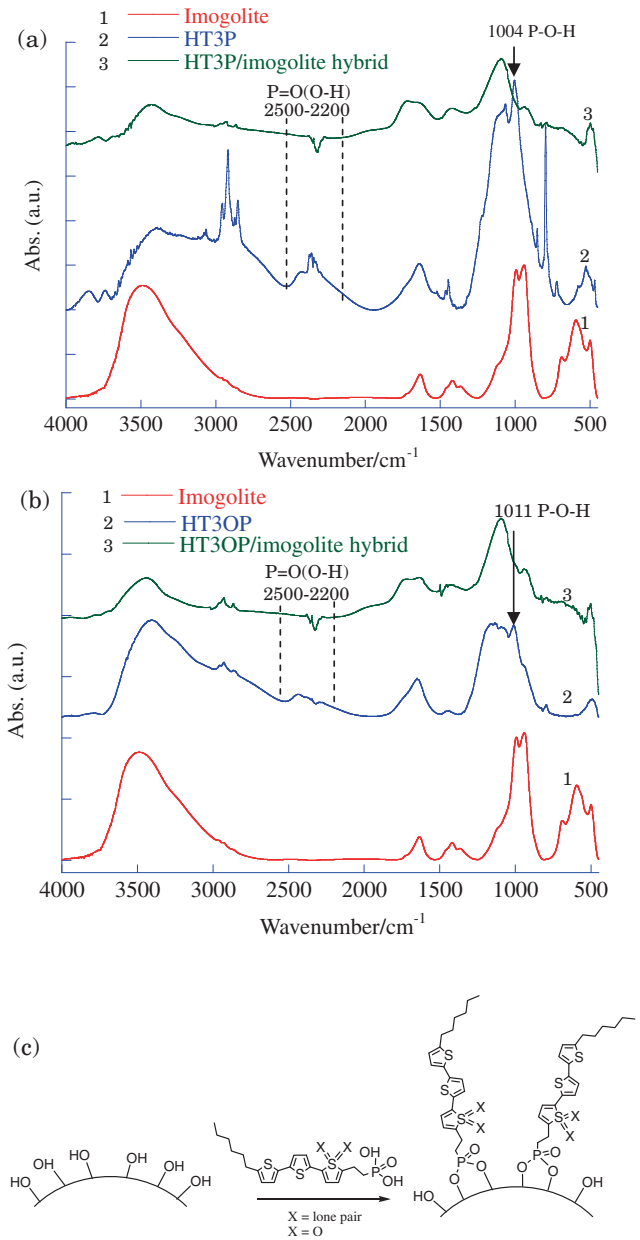

Figure 1. FTIR spectra of (a) HT3P/imogolite hybrid, HT3P, and imogolite, (b) of HT3OP/imogolite hybrid, HT3OP, and imogolite, (c) chemisorption of terthiophenes on imogolite surface.

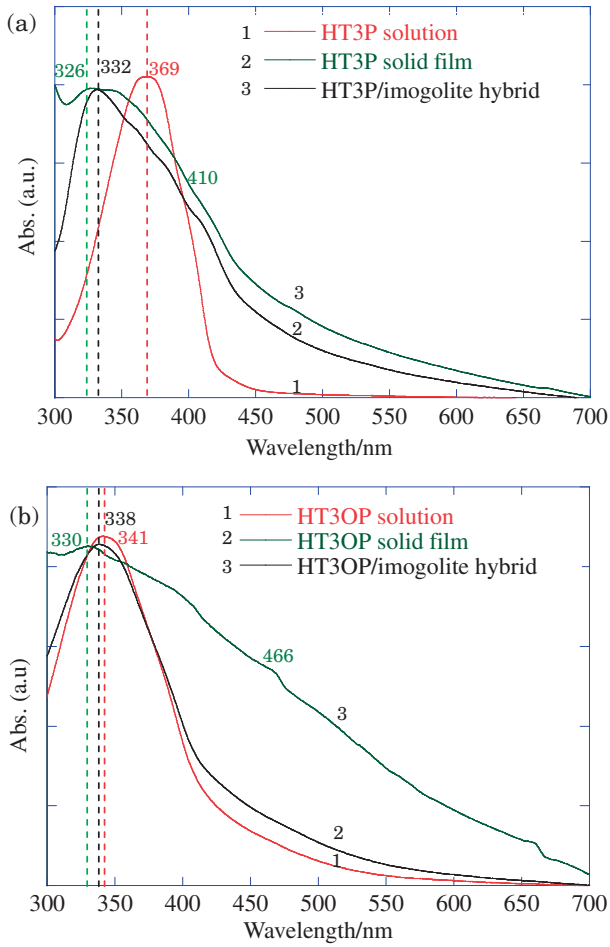

Figure 2. Normalized solid state (cast film), imogolite hybrid, and solution absorption spectra of (a) HT3P and (b) HT3OP.

lite hybrid were compared with their solutions and solid-state counterparts as shown in Figure 2. HT3P and HT3OP which differ in insertion of S=O groups have different absorption maxima in THF solution.[34] In the solid state (solvent cast film), the spectra of both isomer are blue-shifted to different degrees with significant broadened band. A similar trend in blue shifting behavior is observed in the terthiophene/imogolite hybrid spectra. Two factors contribute to the spectral changes arising upon solidification from solution (adsorbed on quartz plate or imogolite surface): planarity and intermolecular interaction.[40–42] Normally, the molecular backbone is more planar in solid state which leads to corresponding red shifts compared to isolated state in solution due an increase in conjugation length. However, the solid-state spectra of most thiophene-based oligomers are blue-shifted compared to solution which suggest the presence of additional intermolecular interaction that may play a role in controlling the solid-state optical properties.[41] Both HT3P and HT3OP when adsorbed on imogolite surface display a solid-state blue shifting absorption indicating H-aggregation. When two interacting molecules have their long axes parallel to each other, the coupling between the transition dipole leads to Davydov splitting of the excited level into two exciton bands, in which the low-energy transitions are forbidden.[43] The small shoulder observed experimentally in the solid-state spectra at relatively long wavelength correspond to these low energy transitions (410 nm for HT3P and 466 nm for HT3OP), while the major absorption bands observed in the solid-state spectra correspond to the allowed high energy transitions of interacting molecules. For the spectra of terthiophene/imogolite hybrid, the shift between solid-state and solution spectra in HT3OP/imogolite hybrid is less dramatic than those in the HT3P/imogolite hybrid. Introduction of S=O groups into the HT3OP leads to weaker intermolecular interaction (π–π interaction) causing lower extent of H-aggregation of HT3OP in solid state (on quartz plate and imogolite surface).

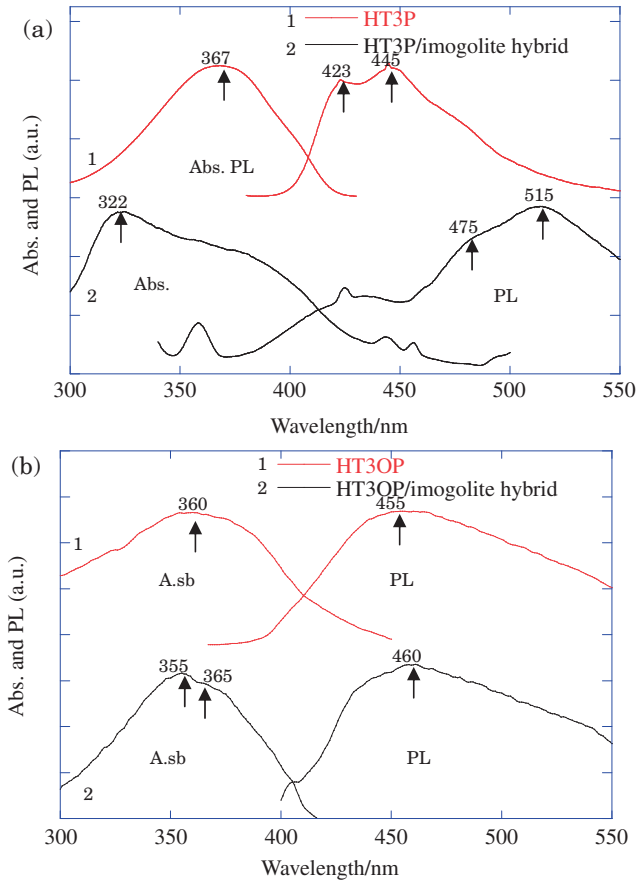

Figure 3. Fluorescence excitation/emission spectra of (a) HT3P, HT3P/imogolite hybrid and (b) HT3OP, HT3OP/imogolite hybrid. The emission wavelength monitored for excitation spectrum and excitation wavelength used for emission spectrum were as follows: (a, 1) $\lambda_{em} = 445$ nm, $\lambda_{ex} = 366$ nm; (a, 2) $\lambda_{em} = 326$ nm, $\lambda_{ex} = 519$ nm. (b, 1) $\lambda_{em} = 455$ nm, $\lambda_{ex} = 360$ nm; (b, 2) $\lambda_{em} = 460$ nm, $\lambda_{ex} = 460$ nm.

Fluorescence Spectroscopy. The optical properties of HT3P, HT3OP, and their imogolite hybrids of HT3P and HT3OP were further investigated by fluorescence spectroscopy. The fluorescence excitation spectra as shown in Figure 3 are found to be identical to the absorption spectra, indicating that the emission is initiated by vertical excitation.[44]

HT3P/imogolite hybrid showed an absorption peak at 322 nm. The peak shift with respect to the HT3P in THF solution ($\lambda_{max} = 367$ nm) can be attributed to the formation of H-type intermolecular interaction when chemisorbed on imogolite as described in the previous section. The fluorescence spectrum has λ_{max} at 515 nm and a shoulder 475 nm. The emission at 515 nm, red-shifted with respect to that of HT3P solution ($\lambda_{max} = 445$ nm), can be attributed to the impact of intermolecular interaction in the hybrid.[45,46] The shoulder at 475 nm indicates the presence of a higher energy emitting states. Nevertheless, the origin of such states as well as minor variation of the spectrum observed in this region is not clear at the moment.

The absorption spectrum of HT3OP/imogolite hybrid resembles that of the HT3OP solution, with λ_{max} at 355 nm; a weak shoulder is observed at ca. 365 nm. The peak shows blue shifting against the HT3OP solution ($\lambda_{max} = 360$ nm) indicating that HT3OP exhibits H-aggregate formation on imogolite surfaces. The fluorescence spectrum of HT3OP/imogolite has λ_{max} at 460 nm and a weak shoulder at around 440 nm. Again the emission peak was red-shifted with respect to that of HT3OP solution ($\lambda_{max} = 455$ nm) suggesting the presence of intermolecular interaction.[45,46] The peaks shifting in the fluorescence spectrum of HT3OP/imogolite is however less significant than that of HT3P/imogolite hybrid. It was speculated that HT3OP forms weaker H-aggregates on imogolite due to the presence S=O in the HT3OP backbone which decreases the planarity and π–π interaction among molecules thus showing less significant peak shifting.

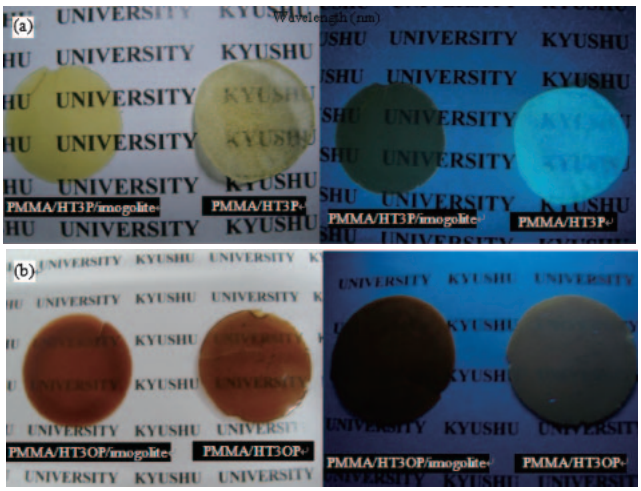

Figure 4. Polymeric film of (a) PMMA/HT3P, PMMA/HT3P/imogolite and (b) PMMA/HT3OP, PMMA/HT3OP/imogolite under visible light (left) and illumination by irradiation at 365 nm (right).

The photoluminescence of HT3P, HT3OP, and their imogolite hybrids in solid state was investigated. 10 wt% of HT3P, HT3P/imogolite, HT3OP, and HT3OP/imogolite were mixed with PMMA solution in THF in order to fabricate polymeric film. The samples were stirred until dissolved completely before transferring to the Petri dish. Placing the Petri dish on a hot plate to remove the solvent will produce PMMA hybrid film with thickness of ca. 0.2 mm. Figure 4 show the polymeric film of PMMA/HT3P, PMMA/HT3P/imogolite, PMMA/HT3OP, and PMMA/HT3OP/imogolite under visible light and illumination by irradiation at 365 nm. Under visible light, both HT3P and HT3P/imogolite PMMA film appeared bright yellowish as shown in Figure 4a. When illuminated by UV irradiation ($\lambda = 365$ nm), judging by naked eye, HT3P showed stronger fluorescence than HT3P/imogolite in PMMA matrix. HT3P/imogolite displays a weak fluorescence in solid state of PMMA film which can be explained in term of formation of HT3P H-aggregate on imogolite surface. The pictures in Figure 4b show that by insertion of S=O moieties into the backbone of HT3P, change of shades in brown can be obtained. Under UV irradiation, a similar trend is observed in the case of HT3OP where it fluoresce stronger than HT3OP/imogolite, an impact of H-aggregation of HT3OP on imogolite surface. In H-aggregate geometric form, the transition momenta of two

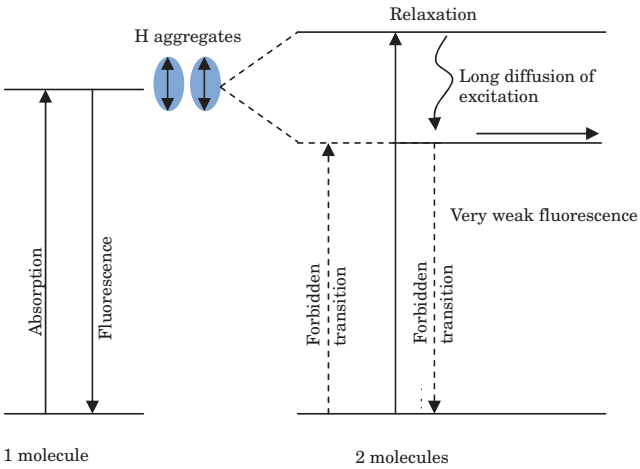

Figure 5. Electronic transition and excitation diffusion of H-aggregate.

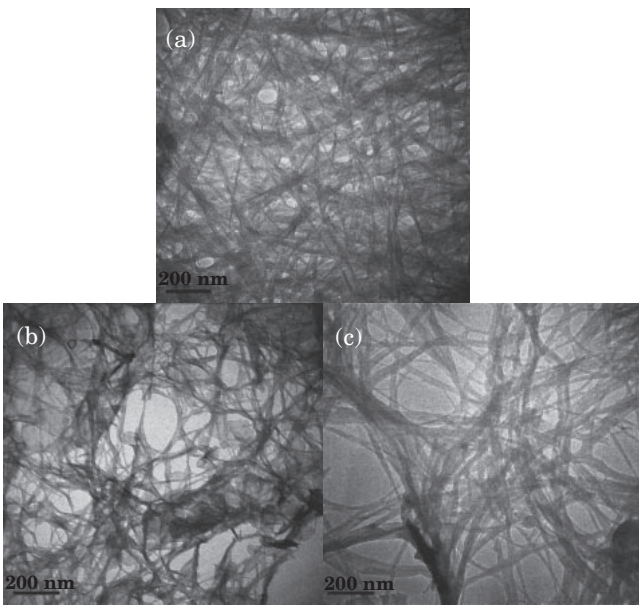

Figure 6. TEM images of (a) imogolite, (b) HT3P/imogolite, and (c) HT3OP/imogolite hybrid. Scale bar is 200 nm.

terthiophene molecules are parallel to each other (Figure 5) and perpendicular to their axis, it is the upper level which corresponds to permitted transition and absorption, and accordingly there is a blue shift. After relaxation from higher to lower level, since the transition to the lower level is forbidden, fluorescence of terthiophene on imogolite is very weak and suppresses any electroluminescence. Nevertheless, once the system is relaxed, the return from excited stated to fundamental states is unlikely and the excitation can diffuse over relatively long distances.[43] This latter property renders HT3P/imogolite and HT3OP/imogolite beneficial for photovoltaic effect where necessary separation of electron and holes is favored by the presence of an electric field.

TEM Observation and Adsorption of Terthiophenes on Imogolite. In order to reveal if terthiophene aggregate did form on imogolite, and to detect if such aggregation could produce any effect on the morphology of imogolite, TEM

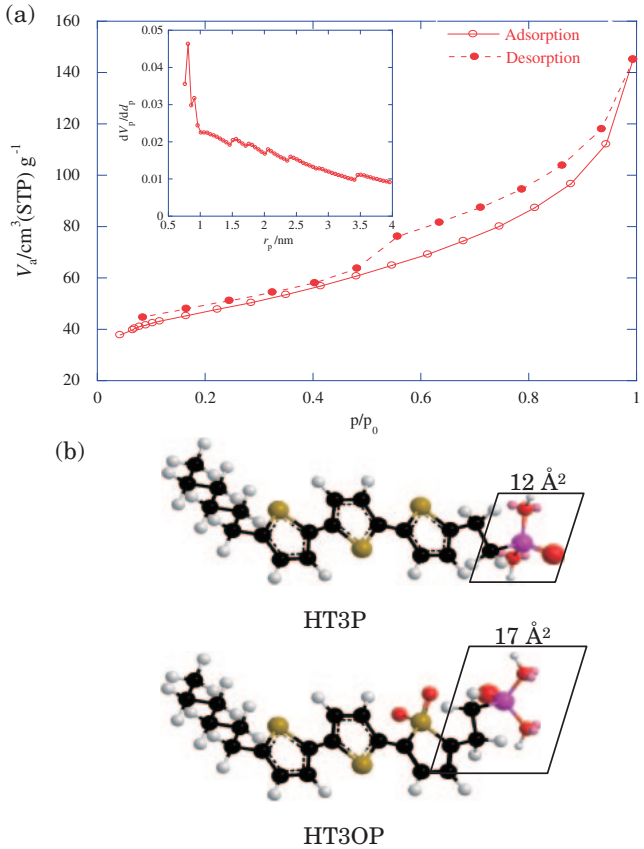

Figure 7. (a) N_2 adsorption–desorption isotherms of imogolite. Inset shows the HK pore-size distribution chart. (b) Area per molecule on imogolite surface.

observations were carried out on imogolite before and after terthiophene chemisorptions. Figure 6a shows the TEM image of a typical example of imogolite fibrous bundles morphology, with each bundle containing many individual imogolite nanotubes.[20–24] The imogolite bundles were entangled forming a dense network of web-like structure. TEM images of imogolite after HT3P and HT3OP adsorption are shown in Figures 6b and 6c, respectively. In both cases, HT3P/imogolite and HT3OP/imogolite were predominantly fibrous, with a network of web structure identical to pristine imogolite. Judging from TEM image, it is very difficult to estimate the near monolayer coverage of terthiophene on imogolite surface. From TEM images of Figures 6b and 6c, the diameter of each bundle was estimated to be ca. 5 to 100 nm which accommodated 2 to 40 terthiophene-modified imogolite nanotubes.

The microporous structure of synthetic imogolite was investigated by nitrogen adsorption–desorption measurement. The nitrogen adsorption–desorption isotherms (Figure 7) agree well with previous adsorption studies on synthetic imogolite, with a type-H3 loop attributed to adsorbate condensation in open slit-shaped pore of imogolite tubes.[47,48] From BET plot (not shown), the BET specific surface area and pore volume is 171.1 $m^2 g^{-1}$ and 0.2 $cm^3 g^{-1}$, respectively. The pore size distribution based on HK model shows a narrow distribution of pore sizes centered at pore diameter of 0.81 nm (Figure 7 inset). The pore size distribution is monomodal which indicates a monodisperse diameter and uncapped structures of imogolite

porous system with no mesoporosity (pore diameter of 2 to 50 nm) associated with the packing of imogolite tube bundles.

Nevertheless, the exact values of the pore size as reported by previous study should be taken with caution, being based on a number of assumptions regarding the pore geometry, packing of nitrogen in the pore, and slight variation in imogolite geometry batch by batch.[49,50] It should be noted that during chemisorptions in solution, terthiophenes do not have full access to the internal pores of imogolite which are occupied by solution coupled by the limitation of internal pore size of imogolite which is smaller than terthiophene (0.5–2.1 nm based on CPK model estimation). With these assumptions, the chemisorptions of terthiophene will mainly occur on the surface of imogolite. Assuming that the concentration of monomeric terthiophene on imogolite surface is negligibly small, the equilibrium concentration of terthiophene adsorbed on imogolite surface was spectrometrically determined to be the following,[51]

$$[\text{Terthiophene}]_{ad} = ([\text{Terthiophene}]_{init} - [\text{Terthiophene}])V/S \quad (1)$$

where $[\text{Terthiophene}]_{init}$ (the subscript "$_{init}$" denotes initial concentration) and $[\text{Terthiophene}]_{ad}$ calculated from UV–vis spectra. S and V are the total surface area of the imogolite (BET specific surface area) and the volume of the solution, respectively. The obtained equilibrium concentration of terthiophenes of HT3P and HT3OP on imogolite surface is 6.0 and 4.5 mg m^{-2}, respectively. Using the above value, the area per molecule on imogolite surface was calculated to be ca. 12 $Å^2$/molecule for HT3P and ca. 17 $Å^2$/molecule for HT3OP. The HT3OP with the S=O in thiophene ring has larger molecular occupied area than HT3P. Such a tendency clearly indicates that intermolecular interaction between molecules contributes to the adsorption behavior of terthiophenes on imogolite surface.

Current–Voltage Characteristics of Imogolite and Their Hybrids. Imogolite has been conceived as an insulator with a wide band gap since the outer and inner wall of imogolite nanotubes consist of wide band gap insulating materials, i.e., alumina and silica, respectively. According to previous results reported by Park et al., imogolite behaves like an insulator under vacuum.[52] They discovered that current flow occurred on the surface of imogolite only after adsorption of water, while no current flow through imogolite was observed if imogolite was exposed to other gases and organic compounds such as O_2, N_2, Ar, benzene, ethanol, and pyridine. The current flow observed was attributed to the ability of OH groups on imogolite surface to lose or gain positive charge (proton) from aqueous solution resulting in net change of surface charge. At low pH values, the net charge of the surface is positive and is negative at high pH values. This can be shown by the following two chemical reactions.[52]

$$\equiv\text{AlOH} + \text{H}^+ \rightleftharpoons [\text{AlOH}_2]^+ \quad (2)$$

$$\equiv\text{AlOH} \rightleftharpoons \text{AlO}^- + \text{H}^+ \quad (3)$$

It was reported that the pH point of zero charge i.e., pH value where net charge between $[\text{AlOH}_2]^+$ and AlO^- is zero for pristine imogolite is around 9.[53] Below pH 9 the positively charged surface species $[\text{AlOH}]^+$ which is believed to have a role in surface conduction predominates. Additionally, Park et al. studied the *I–V* curve measured at varying gate voltage (V_G) and determined p-type characteristic of water/imogolite system.[53] Although the real mechanism is not clear at the moment, it is speculated that an effective motion of this positive charge along imogolite surface will contribute to an increased in current transfer.

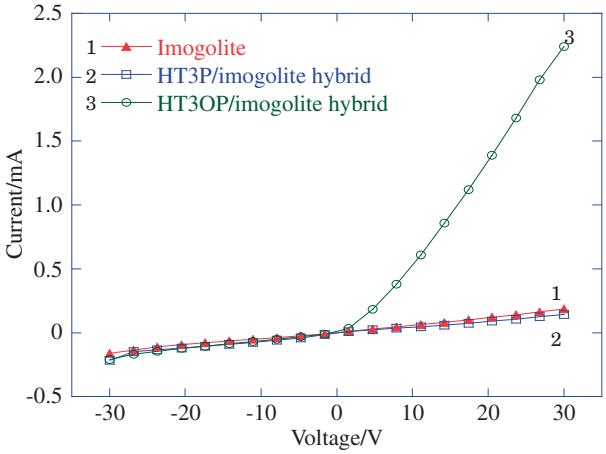

Figure 8. *I–V* curves of imogolite, HT3P/imogolite, and HT3OP/imogolite hybrid.

Figure 8 shows the plots of current of the order of milliamperes versus applied bias voltage give *I–V* curves in the voltage range −30–30 V. Clearly, the *I–V* curve of imogolite in our system does not show an insulator behavior, with current flow observed and the average electrical conductance calculated from forward bias region was 5.9 μS. The current flow was believed to be due to bound water molecules between imogolite tubes which are usually difficult to remove simply by vacuum. The *I–V* curve of HT3OP/imogolite appears non-ohmic. This may be attributed to the disordered packing of HT3OP on imogolite behaving like semiconductor or metal–semiconductor Schottky junction. Surprisingly, the electrical conductance of HT3OP/imogolite increased to 60.8 μS, which is one order of magnitude greater than that of pristine imogolite. It was speculated that OH replaced by terthiophene will consequently reduces positive charge concentration, and suppress p-type behavior. It must be noted that HT3OP is considered a electron acceptor when interacting with imogolite, with the S=O of HT3OP in thiophene withdrawing negative charge from imogolite causing effective motion of positive charges on imogolite surface. HT3OP introduced onto the surface of the imogolite that serves as an electron acceptor to contribute to amplified p-type conductivity; this process is similar to the chemical doping of carbon nanotubes with alkaline metal.[54–57] Similar explanation can be applied for *I–V* behavior observed in the case of HT3P/imogolite. The electrical conductance of HT3P/imogolite estimated from forward bias region is 4.5 μS, which is lower than that of before HT3P doping. In this case, HT3P which acts as an electron donor when interacting with imogolite, with the sulfur atom of the HT3P thiophene ring transferring negative charge to imogolite, hamper the effective motion of positively charged surface species on imogolite surface, and thus reduced the p-type conductivity of imogolite.

Conclusion

In summary, we presented a rational design for the preparation of dye/imogolite hybrid mediated by phosphonic acid moiety that acts as an anchoring group. Use of unsubstituted and substituted terthiophenes has allowed us to study the effect of the substitution and the intermolecular interactions on the optical and photophysical properties of these molecules when chemisorbed on imogolite surface. Following the chemisorption on imogolite surface or in solid state, HT3P exhibits a substantial Davydov splitting, suggesting the strong π–π interactions between molecules in the condensed phase, which leads to an important blue shift of the allowed transition with respect to monomeric HT3P. In contrast, less significant optical changes are observed following the chemisorptions on imogolite or in solid state for HT3OP. Indeed, only small blue shift is observed in the absorption (or excitation) spectra, which clearly shows that intermolecular interactions are weak for this molecule in the condensed phase. The UV–vis spectra in addition to diminished fluorescence indicate that both HT3P and HT3OP adopt H-aggregate geometric form on imogolite surface. An enhanced conductivity of imogolite is observed when chemisorbed by electron-withdrawing HT3OP. The real mechanism behind such enhancement is not clear. Further investigation of these phenomena may also help us to increase our still poor understanding of the effect of doping on electronic properties of imogolite.

Experimental

Synthesis of Imogolite. Imogolite was synthesized according to a method developed by Farmer et al.[21] An aqueous solution of aluminum chloride [$AlCl_3 \cdot 6H_2O$] was mixed with an aqueous solution of tetraethoxysilane $Si(OEt)_4$. The final concentration of the solution was 2.4 mmol L^{-1} with respect to Al and 1.4 mmol L^{-1} for Si. The mixture was stirred for an hour in order to completely hydrolyze the $Si(OEt)_4$. Aqueous NaOH (0.1 mol L^{-1}) was added slowly until the solution reached pH 5. The solution was then reacidified by addition of 1 mmol of HCl and 2 mmol of acetic acid per liter of solution. The solution was then stirred at 369 K for another 4 days. After being cooled to room temperature, the solution was gelated by saturated NaCl solution (8.6 mmol L^{-1}) and rinsed with distilled water using a 100 nm Milipore filter to obtain suspended gel-like material. The rinsed imogolite gel in weak acidic solution was redispersed by sonication. A cotton-like solid imogolite was obtained by freeze-drying the dispersed imogolite solution.

Synthesis of Terthiophene. 2-(5-Bromo-2-thienyl)ethanol (BrTOH), 2-(5″-hexyl-2,2′:5′,2″-terthiophen-5-yl)ethanol (HT3OH), 5-(2-bromoethyl)-5″-hexyl-2,2′:5′,2″-terthiophene (HT3Br), and 2-(5″-hexyl-2,2′:5′,2″-terthiophen-5-yl)ethylphosphonic acid (HT3P) and their oxidized counterpart of 2-(5-bromo-2-thienyl)ethanol 1,1-dioxide (BrTOOH), 2-(5″-hexyl-2,2′:5′,2″-terthiophen-5-yl)ethanol 1,1-dioxide (HT3OOH), 5-(2-bromoethyl)-5″-hexyl-2,2′:5′,2″-terthiophene 1,1-dioxide (HT3OBr), and 2-(5″-hexyl-2,2′:5′,2″-terthiophen-5-yl)ethylphosphonic acid 1,1-dioxide (HT3OP) were synthesized according to a previously described method.[34–36,58–60]

Synthesis of HT3P: 2-(5-Bromo-2-thienyl)ethanol (BrTOH); Under N_2 atmosphere, to a solution of 2-(2-thienyl)ethanol (2.56 g, 20 mmol) in toluene was added stepwise NBS (3.56 g, 20 mmol). The solution was then stirred for 2 h at 253 K in the dark. After being warmed back to room temperature, the solution was stirred overnight. To the resulting solution was added 10% KOH solution in order to neutralize the acidic solution. The reaction mixture was extracted 3 times and the organic layer was dried with anhydrous $MgSO_4$. The solvent was removed by rotary evaporation and the product of BrTOH in colorless liquid (4.08 g, 98.5%) was ready for the next reaction. ^{1}H NMR (400 MHz, $CDCl_3$, Me_4Si): δ 3.00 (2H, t, $J = 6.2$ Hz, CH_2), 3.84 (2H, t, $J = 6.2$ Hz, CH_2), 6.64 (1H, d, $J = 3.6$ Hz, thiophene ring proton), 6.89 (1H, d, $J = 3.6$ Hz, thiophene ring proton).

2-(5″-Hexyl-2,2′:5′,2″-terthiophen-5-yl)ethanol (HT3OH); To a solution of BrTOH (2.49 g, 12 mmol) and 400 mg of [$Pd(PPh_3)_4$] in THF, 5′-hexyl-2,2′-bithiophen-5-ylboronic acid pinacol ester (4.56 g, 12.1 mmol) and 126 mL of saturated $NaHCO_3$ was mixed together and stirred overnight at 353 K in the dark. The resulting solution was extracted with saturated NaCl aqueous solution and diethyl ether, and the organic layer was dried with anhydrous $MgSO_4$. After the solvent was removed by rotary evaporation, the crude product was purified by column chromatography on silica gel with CH_2Cl_2 and the yellow powder of HT3OH (2.06 g, 45.5%) was obtained after being recrystallized from THF and methanol. ν_{max}(film)/cm^{-1} 3247 (OH), 3066 (CH arom), 2954–2856 (CH aliph), 1522 (C=C arom), 1466–1446 (C–H aliph), 1048 (CS arom), 795 (thiophene); ^{1}H NMR (400 MHz, $CDCl_3$, Me_4Si): δ 0.89 (3H, t, $J = 7.0$ Hz, CH_3), 1.26–1.43 (6H, m, $3 \times CH_2$), 1.68 (2H, m, CH_2), 2.79 (2H, t, $J = 7.7$ Hz, CH_2), 3.05 (2H, t, $J = 6.0$ Hz, CH_2), 3.88 (2H, q, $J = 5.9$ Hz, CH_2), 6.68 (1H, d, $J = 3.6$ Hz, thiophene ring proton), 6.78 (1H, d, $J = 3.5$ Hz, thiophene ring proton), 6.98 (2H, dd, $J = 3.9$ and 2.5 Hz, thiophene ring protons), 7.03 (2H, d, $J = 3.8$ Hz, thiophene ring protons); ^{13}C NMR (400 MHz, $CDCl_3$, Me_4Si); δ 12.2, 20.7, 26.9, 28.3, 29.7, 31.7, 61.4, 121.4, 121.6, 121.9, 122.9, 124.6, 132.6, 134.6, 138.2, 143.6.

5-(2-Bromoethyl)-5″-hexyl-2,2′:5′,2″-terthiophene (HT3Br); Under N_2 atmosphere, to a solution of HT3OH (2.03 g, 5.4 mmol) in chloroform was added dropwise PBr_3 (0.8 mL, 8.53 mmol) and the mixture was stirred overnight at room temperature in the dark. To the resulting solution, saturated $NaHCO_3$ was added in order to neutralize hydrobromic acid and phosphorus acid. The reaction mixture was extracted 3 times and the organic layer was dried with anhydrous $MgSO_4$. The solvent was removed by rotary evaporation and the yellow solid of HT3Br (0.962 g, 40.6%) was recovered. ^{1}H NMR (400 MHz, $CDCl_3$, Me_4Si): δ 0.85 (3H, t, $J = 6.8$ Hz, CH_3), 1.28 (6H, m, $3 \times CH_2$), 1.58 (2H, m, CH_2), 2.77 (2H, t, $J = 7.5$ Hz, CH_2), 3.32 (2H, t, $J = 7.5$ Hz, CH_2), 3.72 (2H, t, $J = 7.3$ Hz, CH_2), 6.80 (2H, dd, $J = 3.4$ and 0.7 Hz, thiophene ring protons), 6.93 (2H, dd, $J = 3.9$ and 0.6 Hz, thiophene ring protons), 7.11 (2H, dd, $J = 3.5$ and 0.5 Hz, thiophene ring protons).

2-(5″-Hexyl-2,2′:5′,2″-terthiophen-5-yl)ethylphosphonic Acid (HT3P); Under N_2 atmosphere, the reactant of HT3Br (2.49 g, 12 mmol) and tris(trimethylsilyl) phosphite (2 mL,

5.96 mmol) was mixed together and stirred overnight at 423 K in the dark. After the reaction solution was cooled to room temperature, 20 mL of water/methanol (1:1) mixture and stirring continued for another 24 h. The solvent was removed by rotary evaporation and the crude product was purified by being recrytallized from THF and hexane to afford yellow solid of HT3P (1.13 g, 117%). ν_{max}(film)/cm^{-1} 3392 (OH), 3066 (CH arom), 2957–2853 (CH aliph), 2432–2346 (POH), 1520 (C=C arom), 1464–1447 (CH aliph), 1121–1065 (P=O), 797 (thiophene). ^{1}H NMR (400 MHz, $CDCl_3$, Me_4Si): δ 0.85 (3H, t, $J = 5.9$ Hz, CH_3), 1.29 (6H, m, 3 × CH_2), 1.60 (2H, m, CH_2), 2.76 (2H, t, $J = 7.5$ Hz, CH_2), 2.93 (2H, m, CH_2), 3.59 (2H, t, $J = 7.7$ Hz, CH_2), 6.79 (2H, d, $J = 3.5$ Hz, thiophene ring protons), 6.86 (2H, d, $J = 3.7$ Hz, thiophene ring protons), 7.10 (2H, d, $J = 3.6$ Hz, thiophene ring protons).

Synthesis of HT3OP: 2-(5-Bromo-2-thienyl)ethanol 1,1-Dioxide (BrTOOH); BrTOH (6.88 g, 33 mmol) was dissolved in 40 mL of CH_2Cl_2 and the solution added to a mixture of *m*-chloroperbenzoic acid (20.7 g, 70% max, 84 mmol) in 80 mL of CH_2Cl_2. The mixture was stirred overnight at room temperature. The mixture was treated with $NaHCO_3$, dried over $MgSO_4$, solvent removed, and was crystallized from hexane to give (4.98 g, 62%) of BrTOOH as white solid. ^{1}H NMR (400 MHz, $CDCl_3$, Me_4Si): δ 2.80 (2H, t, $J = 5.9$ Hz, CH_2), 3.97 (2H, t, $J = 5.9$ Hz, CH_2), 6.59 (1H, d, $J = 4.8$ Hz, thiophene ring proton), 6.80 (1H, d, $J = 4.8$ Hz, thiophene ring proton).

2-(5″-Hexyl-2,2′:5′,2″-terthiophen-5-yl)ethanol 1,1-Dioxide (HT3OOH); To a solution of BrTOOH (4.98 g, 20.8 mmol) and 400 mg of [Pd(PPh$_3$)$_4$] in THF, 5′-hexyl-2,2′-bithiophen-5-ylboronic acid pinacol ester (8.09 g, 21.5 mmol) and 126 mL of saturated $NaHCO_3$ was mixed together and stirred overnight at 353 K in the dark. The resulting solution was extracted with saturated NaCl aqueous solution and diethyl ether, and the organic layer was dried with anhydrous $MgSO_4$. After the solvent was removed by rotary evaporation, the crude product was purified by column chromatography on silica gel using a graduated solvent of a) 50:50 CH_2Cl_2:hexane, b) 80:20 ethyl acetate:hexane. A total (2.99 g, 35.2%) of HT3OOH was isolated as an orange solid. ν_{max}(film)/cm^{-1} 3446 (OH), 3068 (CH arom), 2924–2852 (CH aliph), 1614, 1508 (C=C arom), 1466–1436 (C–H aliph), 1295, 1138 (S=O), 1033 (CS arom), 795 (thiophene); ^{1}H NMR (400 MHz, $CDCl_3$, Me_4Si): δ 0.89 (3H, t, $J = 5.9$ Hz, CH_3), 1.24–1.33 (6H, m, 3 × CH_2), 1.68 (2H, m, CH_2), 2.80 (2H, t, $J = 6.9$ Hz, CH_2), 2.85 (2H, t, $J = 5.9$ Hz, CH_2), 3.98 (2H, t, $J = 5.5$ Hz, CH_2), 6.55 (1H, d, $J = 5$ Hz, thiophene ring proton), 6.64 (1H, d, $J = 4.7$ Hz, thiophene ring proton), 6.71 (1H, d, $J = 3.7$ Hz, thiophene ring proton), 7.05 (1H, d, $J = 3.5$ Hz, thiophene ring proton), 7.09 (1H, d, $J = 3.9$ Hz, thiophene ring proton), 7.47 (1H, d, $J = 3.9$ Hz, thiophene ring proton); ^{13}C NMR (400 MHz, $CDCl_3$, Me_4Si): δ 11.9, 20.4, 22.7, 26.6, 26.7, 28.0, 29.3, 57.9, 114.3, 121.8, 122.7, 123.0, 123.5, 125.3, 127.0, 131.8, 134.3, 137.7, 138.8, 145.2.

5-(2-Bromoethyl)-5″-hexyl-2,2′:5′,2″-terthiophene 1,1-Dioxide (HT3OBr); Under N_2 atmosphere, to a solution of HT3OOH (1 g, 2.4 mmol) in chloroform was added dropwise PBr_3 (0.35 mL, 3.75 mmol) and the mixture was stirred overnight at room temperature in the dark. To the resulting solution, saturated $NaHCO_3$ was added in order to neutralize hydrobromic acid and phosphorus acid. The reaction mixture was extracted 3 times and the organic layer was dried with anhydrous $MgSO_4$. The solvent was removed by rotary evaporation and the dark range solid of HT3OBr (0.609 g, 52.8%) was recovered. ^{1}H NMR (400 MHz, $CDCl_3$, Me_4Si): δ 0.89 (3H, t, $J = 6.0$ Hz, CH_3), 1.29–1.40 (6H, m, 3 × CH_2), 1.68 (2H, m, CH_2), 2.80 (2H, t, $J = 7.5$ Hz, CH_2), 3.14 (2H, t, $J = 6.8$ Hz, CH_2), 3.68 (2H, t, $J = 6.8$ Hz, CH_2), 6.52 (1H, dd, $J = 29$ and 2 Hz), 6.67 (1H, d, $J = 4$ Hz), 6.70 (1H, d, $J = 4$ Hz), 7.04 (1H, qd, $J = 7$ and 2 Hz, thiophene ring proton), 7.07 (1H, dd, $J = 14$ and 4 Hz, thiophene ring proton), 7.50 (1H, dd, $J = 10$ and 4 Hz, thiophene ring proton).

2-(5″-Hexyl-2,2′:5′,2″-terthiophen-5-yl)ethylphosphonic Acid 1,1-Dioxide (HT3OP); Under N_2 atmosphere, HT3OBr (0.6 g, 1.29 mmol) and tris(trimethylsilyl) phosphite (2.2 mL, 6.45 mmol) were mixed together and stirred overnight at 423 K in the dark. After the reaction solution was cooled to room temperature, 20 mL of water/methanol (1:1) mixture was added and stirring continued for another 24 h. The solvent was removed by rotary evaporation and the crude product was purified by recrytallization from THF and hexane to afford (0.5 g, 82%) dark red solid of HT3OP. ν_{max}(film)/cm^{-1} 3298 (O–H), 3073 (C–H arom), 2955–2857 (C–H aliph), 2382–2279 (PO–H), 1458–1440 (C–H aliph), 1297, 1131 (S=O), 1054 (P=O), 797 (thiophene); ^{1}H NMR (400 MHz, CD_3OD, Me_4Si): δ 0.80 (3H, t, $J = 6.8$ Hz, CH_3), 1.16–1.30 (6H, m, 3 × CH_2), 1.56 (2H, m, CH_2), 1.76 (2H, t, $J = 6.4$ Hz, CH_2), 2.69 (2H, t, $J = 7.2$ Hz, CH_2), 3.62 (2H, t, $J = 6.5$ Hz, CH_2), 6.61 (2H, td, $J = 12$ and 4 Hz, thiophene ring protons), 6.82 (1H, d, $J = 1$ Hz, thiophene ring proton), 6.92 (1H, d, $J = 9$ and 4 Hz, thiophene ring proton), 6.98 (1H, dt, $J = 6$ and 2 Hz, thiophene ring proton), 7.03 (1H, dd, $J = 9$ and 4 Hz, thiophene ring proton).

Preparation of Terthiophene/Imogolite Hybrid Materials. To a low acidic aqueous imogolite solution (12 mL, 1 mg mL^{-1}) was added dropwise a THF solution of HT3P (12 mL, 1 mg mL^{-1}) and the mixture was stirred overnight at room temperature in the dark. The weight ratio of imogolite and HT3P was 1:1. The suspended solution was centrifuged (12000 rpm, 15 min) to obtain HT3P/imogolite precipitate. The supernatant was decanted followed by addition of the same amount of fresh THF. The decanting, addition of THF and centrifugation were repeated 3 times to rinse out weakly or nonchemisorbed HT3P. The precipitate was finally redispersed in distilled water for freeze drying. Freeze drying the precipitate resulting in cotton-like yellow solid. The same procedure was applied for HT3OP to produce cotton-like pale brown solid of HT3OP/imogolite hybrid. For comparison, a similar procedure was applied for terthiophenes of OH group derivatives (HT3OH and HT3OOH) to test their adsorption on imogolite surface. However, no precipitate perceptible to the naked eye occurred in the case of HT3OH/imogolite and HT3OOH/imogolite suspended solution after centrifugation (Figure 9).

Characterization. ^{1}H NMR and ^{13}C NMR spectra were taken on a JNM-EX-400 (JEOL, Japan) 400 MHz spectrometer. IR spectra were recorded as KBr pellets using Spectrum One

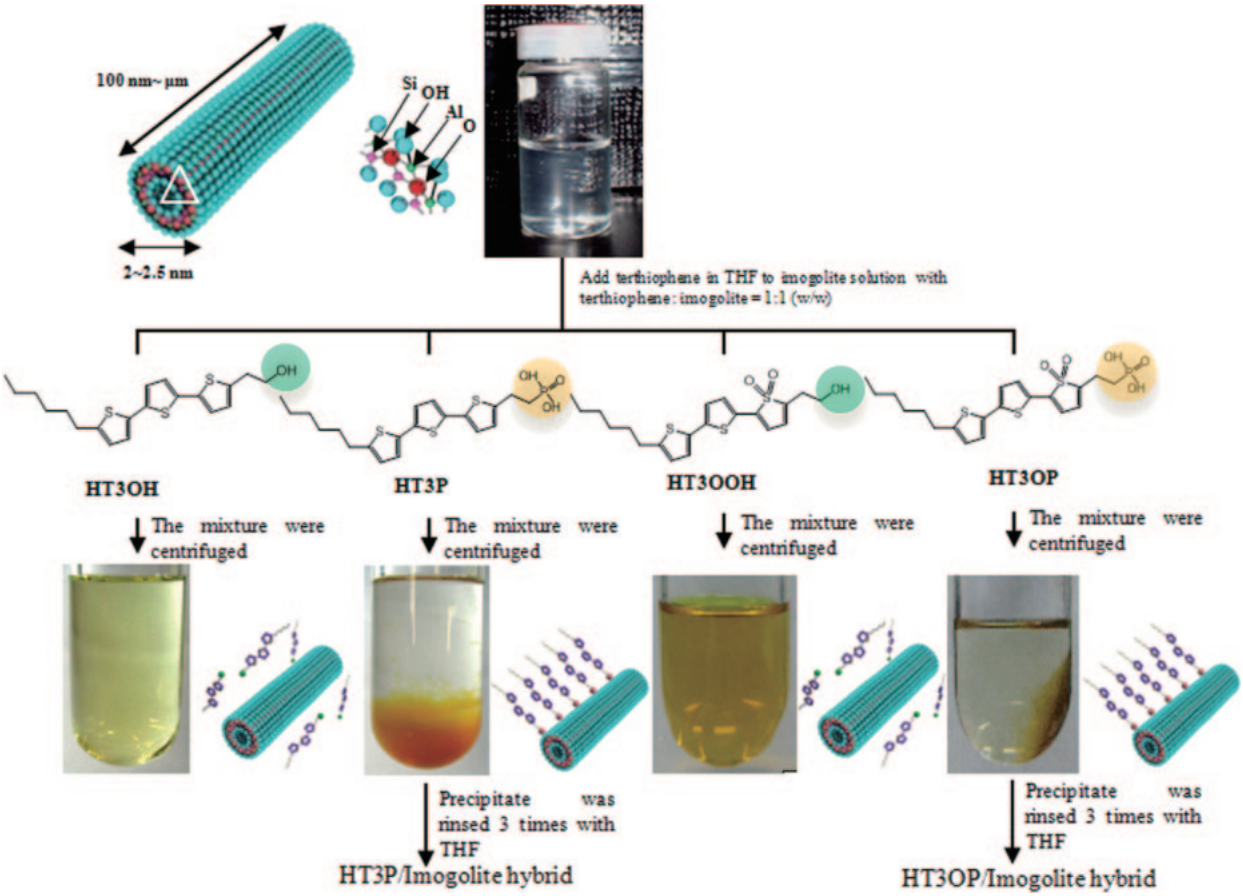

Figure 9. Schematic illustration of imogolite structure and the preparation of terthiophene/imogolite hybrid materials.

(Perkin-Elmer Japan Co., Ltd.) with a resolution of 0.5 cm^{-1} at room temperature. IR data were collected by averaging 16 scans between 4000 and 450 cm^{-1}. UV–visible absorption spectroscopy was performed on a Shimadzu UV-3600 UV–vis–NIR spectrophotometer. Fluorescence excitation and emission spectra were recorded on a FP-6600 spectrofluorometer. The films of compound HT3P and HT3OP were prepared by drop casting THF solutions onto quartz slides at room temperature. After taking the solid-state spectra, the films dissolved in THF, and their UV–vis spectra were compared to the freshly prepared solution. The TEM images of imogolite before and after dye adsorption were taken using a H-7500 instrument (Hitachi, Japan) operating under acceleration voltage of 100 kV. The TEM samples were prepared by applying imogolite solution onto a copper grid covered with carbon film. Nitrogen adsorption–desorption isotherms were recorded on a Belsorp 18Plus-SP instrument (Japan Bell Inc.) at 77 K in the relative pressure range from 0.1 to 0.99. The Brunauer–Emmett–Teller (BET) surface areas were obtained from data under relative pressure between 0.05 and 0.30. For the current–voltage (*I–V*) measurements, two gold electrodes separated by 1.5 mm were magnetically sputtered on a silicon wafer. The samples with exposed area of ca. 0.8 cm^2 were deposited between the electrodes. *I–V* curves were measured in vacuum at 25 °C with an Agilent E5272A source monitor unit. *I–V* curves were plotted by Metrics IC/V software.

This work was supported by a Grant-in-Aid for the Global COE Program, "Science for Future Molecular Systems" (No. 1520258), and Grant-in-Aid for Scientific Research A (No. 19205031) from the Ministry of Education, Culture, Sports, Science and Technology of Japan.

References

1 M.-C. Daniel, D. Astruc, *Chem. Rev.* **2004**, *104*, 293.
2 A. C. Khazraji, S. Hotchandani, S. Das, P. V. Kamat, *J. Phys. Chem. B* **1999**, *103*, 4693.
3 G. McDermott, S. M. Prince, A. A. Freer, A. M. Hawthornthwaite-Lawless, M. Z. Papiz, R. J. Cogdell, N. W. Isaacs, *Nature* **1995**, *374*, 517.
4 J. M. Olson, *Photochem. Photobiol.* **1998**, *67*, 61.
5 J.-P. Zhang, R. Fujii, P. Qian, T. Inaba, T. Mizoguchi, Y. Koyama, K. Onaka, Y. Watanabe, H. Nagae, *J. Phys. Chem. B* **2000**, *104*, 3683.
6 W. O. Yah, Z. Wang, H. Otsuka, K. Kato, J. Kim, M. Takata, A. Takahara, *ACS Appl. Mater. Interfaces* **2009**, *1*, 1544.
7 Q. Zhang, T. Atay, J. R. Tischler, M. S. Bradley, V. Bulovic, A. V. Nurmikko, *Nat. Nanotechnol.* **2007**, *2*, 555.
8 M. Murai, A. Furube, M. Yanagida, K. Hara, R. Katoh, *Chem. Phys. Lett.* **2006**, *423*, 417.
9 E. Galoppini, *Coord. Chem. Rev.* **2004**, *248*, 1283.
10 M. Linke-Schaetzel, A. D. Bhise, H. Gliemann, T. Koch, T. Schimmel, T. S. Balaban, *Thin Solid Films* **2004**, *451–452*, 16.

11 L. Daehne, K. Kamiya, J. Tanaka, *Bull. Chem. Soc. Jpn.* **1992**, *65*, 2328.
12 I. Place, J. Perlstein, T. L. Penner, D. G. Whitten, *Langmuir* **2000**, *16*, 9042.
13 X. Marguerettaz, R. O'Neill, D. Fitzmaurice, *J. Am. Chem. Soc.* **1994**, *116*, 2629.
14 X. Marguerettaz, D. Fitzmaurice, *J. Am. Chem. Soc.* **1994**, *116*, 5017.
15 P. Péchy, F. P. Rotzinger, M. K. Nazeeruddin, O. Kohle, S. M. Zakeeruddin, R. Humphry-Baker, M. Grätzel, *J. Chem. Soc., Chem. Commun.* **1995**, 65.
16 S. M. Zakeeruddin, M. K. Nazeeruddin, P. Pechy, F. P. Rotzinger, R. Humphry-Baker, K. Kalyanasundaram, M. Grätzel, V. Shklover, T. Haibach, *Inorg. Chem.* **1997**, *36*, 5937.
17 I. Gillaizeau-Gauthier, F. Odobel, M. Alebbi, R. Argazzi, E. Costa, C. A. Bignozzi, P. Qu, G. J. Meyer, *Inorg. Chem.* **2001**, *40*, 6073.
18 E. Bae, W. Choi, J. Park, H. S. Shin, S. B. Kim, J. S. Lee, *J. Phys. Chem. B* **2004**, *108*, 14093.
19 M. Nilsing, S. Lunell, P. Persson, L. Ojamäe, *Surf. Sci.* **2005**, *582*, 49.
20 N. Yoshinaga, S. Aomine, *Soil Sci. Plant Nutr.* **1962**, *8*, 22.
21 V. C. Farmer, A. R. Fraser, J. M. Tait, *J. Chem. Soc., Chem. Commun.* **1977**, 462.
22 P. D. G. Cradwick, V. C. Farmer, J. D. Russell, C. R. Masson, K. Wada, N. Yoshinaga, *Nature (London), Phys. Sci.* **1972**, *240*, 187.
23 K. Yamamoto, H. Otsuka, S.-I. Wada, A. Takahara, *Chem. Lett.* **2001**, 1162.
24 K. Wada, *Minerals in Soil Environments*, 2nd ed., ed. by J. B. Dixon, S. B. Weed, Soil Science Society of America, Madison, Wisconsin, U.S.A. **1989**.
25 X. Marguerettaz, G. Redmond, S. N. Rao, D. Fitzmaurice, *Chem.—Eur. J.* **1996**, *2*, 420.
26 Y.-H. Lee, B.-J. Kim, W. Yi, A. Takahara, D.-W. Sohn, *Bull. Korean Chem. Soc.* **2006**, *27*, 1815.
27 N. Jiravanichanun, K. Yamamoto, H. Yonemura, S. Yamada, H. Otsuka, A. Takahara, *Bull. Chem. Soc. Jpn.* **2008**, *81*, 1663.
28 N. Jiravanichanun, K. Yamamoto, A. Irie, H. Otsuka, A. Takahara, *Synth. Met.* **2009**, *159*, 885.
29 G. Horowitz, P. Valat, F. Garnier, F. Kouki, V. Wintgens, *Opt. Mater.* **1998**, *9*, 46.
30 A. J. Mäkinen, I. G. Hill, T. Noda, Y. Shirota, Z. H. Kafafi, *Appl. Phys. Lett.* **2001**, *78*, 670.
31 M. Kimura, T. Yasuda, K. Kishimoto, G. Götz, P. Bäuerle, T. Kato, *Chem. Lett.* **2006**, *35*, 1150.
32 K. Yamamoto, H. Otsuka, S.-I. Wada, D. Sohn, A. Takahara, *Polymer* **2005**, *46*, 12386.
33 K. Yamamoto, H. Otsuka, S.-I. Wada, D. Sohn, A. Takahara, *Soft Matter* **2005**, *1*, 372.
34 G. Barbarella, O. Pudova, C. Arbizzani, M. Mastragostino, A. Bongini, *J. Org. Chem.* **1998**, *63*, 1742.
35 G. Barbarella, L. Favaretto, G. Sotgiu, M. Zambianchi, L. Antolini, O. Pudova, A. Bongini, *J. Org. Chem.* **1998**, *63*, 5497.
36 G. Barbarella, M. Zambianchi, O. Pudova, V. Paladini, A. Ventola, F. Cipriani, G. Gigli, R. Cingolani, G. Citro, *J. Am. Chem. Soc.* **2001**, *123*, 11600.
37 W. Gao, L. Dickinson, C. Grozinger, F. G. Morin, L. Reven, *Langmuir* **1996**, *12*, 6429.
38 J. T. O'Brien, A. C. Zeppenfeld, G. L. Richmond, C. J. Page, *Langmuir* **1994**, *10*, 4657.
39 G. Steiner, V. Sablinskas, O. Savchuk, R. Bariseviciute, E. Jähne, H. J. Adler, R. Salzer, *J. Mol. Struct.* **2003**, *661–662*, 429.
40 A. Facchetti, M.-H. Yoon, C. L. Stern, G. R. Hutchison, M. A. Ratner, T. J. Marks, *J. Am. Chem. Soc.* **2004**, *126*, 13480.
41 X. Zhang, J. P. Johnson, J. W. Kampf, A. J. Matzger, *Chem. Mater.* **2006**, *18*, 3470.
42 X. Zhang, A. J. Matzger, *J. Org. Chem.* **2003**, *68*, 9813.
43 A. Moliton, R. C. Hiorns, *Polym. Int.* **2004**, *53*, 1397.
44 A. Patra, S. P. Anthony, T. P. Radhakrishnan, *Adv. Funct. Mater.* **2007**, *17*, 2077.
45 A. Yassar, G. Horowitz, P. Valat, V. Wintgens, M. Hmyene, F. Deloffre, P. Srivastava, P. Lang, F. Garnier, *J. Phys. Chem.* **1995**, *99*, 9155.
46 H. DiCésare, M. Belletête, E. R. Garcia, M. Leclerc, G. Durocher, *J. Phys. Chem. A* **1999**, *103*, 3864.
47 S. Brunauer, *The Adsorption of Gases and Vapors*, Oxford University Press, Oxford, UK, **1944**.
48 S. Mukherjee, V. M. Bartlow, S. Nair, *Chem. Mater.* **2005**, *17*, 4900.
49 A. Saito, H. C. Foley, *AIChE J.* **1991**, *37*, 429.
50 M. A. Parent, J. B. Moffat, *Langmuir* **1995**, *11*, 4474.
51 K. Adachi, T. Mita, T. Yamate, S. Yamazaki, H. Takechi, H. Watarai, *Langmuir* **2010**, *26*, 117.
52 J. Oh, S. Chang, J. Jang, S. Roh, J. Park, J. Lee, D. Sohn, W. Yi, Y. Jung, S.-J. Kim, *J. Mater. Sci.: Mater. Electron.* **2007**, *18*, 893.
53 J.-H. Park, J.-W. Lee, S.-Y. Chang, T.-H. Park, B.-W. Han, J.-W. Han, W.-K. Yi, *Bull. Korean Chem. Soc.* **2008**, *29*, 1048.
54 R. S. Lee, H. J. Kim, J. E. Fischer, A. Thess, R. E. Smalley, *Nature* **1997**, *388*, 255.
55 V. Z. Mordkovich, M. Baxendale, S. Yoshimura, R. P. H. Chang, *Carbon* **1996**, *34*, 1301.
56 J. Kong, C. Zhou, E. Yenilmez, H. Dai, *Appl. Phys. Lett.* **2000**, *77*, 3977.
57 B. H. Kim, T. H. Park, S. J. Baek, D. S. Lee, S. J. Park, J. S. Kim, Y. W. Park, *J. Appl. Phys.* **2008**, *103*, 096103.
58 M. Melucci, C. Dionigi, G. Lanzani, I. Viola, G. Gigli, G. Barbarella, *Macromolecules* **2005**, *38*, 10050.
59 M. Melucci, G. Barbarella, G. Sotgiu, *J. Org. Chem.* **2002**, *67*, 8877.
60 E. Jaehne, D. Ferse, G. Busch, H.-J. P. Adler, A. Singh, I. K. Varma, *Des. Monomers Polym.* **2002**, *5*, 427.